IEEE Access
Multidisciplinary | Rapid Review | Open Access Journal

Received May 26, 2020, accepted June 1, 2020, date of publication June 5, 2020, date of current version June 17, 2020.

Digital Object Identifier 10.1109/ACCESS.2020.3000238

A Hybrid Dual-Mode Control for Permanent-Magnet Synchronous Motor Drives

WEI WANG, (Senior Member, IEEE), ZHIXIANG LU, WEI HUA, (Senior Member, IEEE), ZHENG WANG, (Senior Member, IEEE), AND MING CHENG, (Fellow, IEEE)

School of Electrical Engineering, Southeast University, Nanjing 210096, China

Corresponding author: Wei Wang (wangwei1986@seu.edu.cn)

This work was supported in part by the National Natural Science Foundation of China under Project 51991380, Project 51977036, and Project 51607038, in part by the Zhishan Young Scholar Plan of Southeast University of China, and in part by the Jiangsu Key Laboratory of Smart Grid Technology and Equipment of China.

ABSTRACT In order to obtain satisfactory transient and steady-state performances, a hybrid dual-mode control (HDMC) is proposed for surface-mounted permanent-magnet synchronous motor drives (PMSMs), which contains two control modes. The first one is the deadbeat predictive control (DBPC) mode, which is only implemented in the transient procedure. The second one is the field-oriented control (FOC) mode, which is mainly implemented in the steady-state operation. Besides, the FOC mode is also implemented in the transient procedure to eliminate the static current error. In the transient procedure, the FOC mode is activated after one-sampling-period implementation of the DBPC mode in the unsaturation state, and the desired voltage vector calculated in this sampling period is assigned as the initialized values of the proportional-integral current controllers in the FOC mode to avoid the switching chattering. When the voltage-source-inverter comes into the saturation state, the DBPC mode will be reactivated immediately. The proposed HDMC inherits the quick response ability of DBPC and the good steady-state performances of FOC. The effectiveness of the proposed HDMC is verified by the experimental results.

INDEX TERMS Model predictive control (MPC), deadbeat predictive control (DBPC), field-oriented control (FOC), permanent-magnet synchronous motor (PMSM).

I. INTRODUCTION

Due to high power factor, high efficiency and high torque-to-inertia ratio, permanent-magnet synchronous motors (PMSMs) have been widely used in motor drives [1]–[5]. So far, a lot of high-performance control methods have been proposed for PMSM drives, and the field-oriented control (FOC) is usually considered as the most effective and reliable one. In the conventional FOC scheme, direct and quadrature currents are independently regulated by two proportional-integral (PI) controllers [6], [7]. On the other hand, model predictive control (MPC) has recently attracted more attentions for the advantages of fast dynamic response, simple modeling, and multi-object control [8]–[11]. Due to the elimination of PI current controllers, MPC has better transient performances than FOC [12].

The associate editor coordinating the review of this manuscript and approving it for publication was Jinquan Xu.

According to the finite control set and the system model, MPC can predict the future behavior of control variables, such as the current, torque, and stator flux [13], [14]. A cost function is designed according to the errors between the reference and predicted values, and the optimal voltage vector can be selected to minimize the cost function [15]. This scheme is usually noted as finite-control-set MPC (FCS-MPC). Existing FCS-MPC schemes can be mainly categorized into model predictive torque control (MPTC) [16] and model predictive current control (MPCC) [17]. In MPTC, torque and stator flux are selected as the control variables, and their errors are combined together to form a cost function. Usually, a weighting factor is required in the cost function, since both the torque and the stator flux have different units [18]. Additionally, the torque and the stator flux usually cannot be measured easily, and they are usually estimated by mathematical observers. In MPCC, the control variables are direct and quadrature axis currents, which can be measured by sensors directly.

Furthermore, the weighting factor can be eliminated in MPCC, since both control variables have same units.

However, FCS-MPC still suffers from several drawbacks. One of the main drawbacks is the heavy computation burden. The control set of FCS-MPC consists of all possible voltage vectors provided by voltage-source-inverters (VSIs), and the computation burden of FCS-MPC depends on the number of voltage vector candidates in the finite control set. For example, seven current predictions and same cost function calculations are required to determine the optimal voltage vector for three-phase motor drives [19]. Furthermore, N^n voltage vectors will be evaluated for an N-level n-phase VSI. Obviously, the computation burden will be significantly increased with more voltage vectors. The heavy computation burden requires longer calculation time, and then reduces the average switching frequency of VSI, especially in multi-phase motor or multi-motor drives. On the other hand, no pulse-width-modulation module is employed in FCS-MPC, and only one basic voltage vector can be implemented by VSI in one sampling period. As a result, the switching frequency of VSI is inconstant, and large ripples of stator flux, electromagnetic torque and stator current will occur [20]. These drawbacks have limited the industrial applications of FCS-MPC.

In order to inherit the advantages but overcome the drawbacks of FCS-MPC, another MPC scheme named as deadbeat predictive control (DBPC) have been proposed, in which the control commands are expected to be achieved in one sampling period [21], [22]. In DBPC, a desired voltage vector is directly calculated by the inverse motor model instead of evaluating all possible voltage vectors, and then the minimizing process is also not required since the cost function has been eliminated [23]–[25]. Therefore, the computation burden of DBPC can be significantly reduced comparing with that of FCS-MPC [26]. According to PWM technique, the desired voltage vector can be synthesized by zero and active voltage vectors in one sampling period. Hence, DBPC has constant switching frequency and can simultaneously achieve good transient and steady-state performances.

As a model-based control method, however, the performances of DBPC highly depend on the accuracy of motor model. As is known, the differences between model parameters and actual parameters usually cannot be avoided in the practical implementation of DBPC, which may be resulted by the measurement errors and the parameter variations. The measurement errors usually depend on the accuracy of sensors. During the operation, the motor parameters can be affected by thermal, deep-bar, and saturation effects. For example, the stator resistance varies with temperature, and the inductance can be influenced by the magnetic saturation and the air gap variation. Due to the heating and vibration of PMSMs, demagnetization of permanent-magnets may occur [27]. Considering the parameter differences, current oscillation and static current errors usually exist [28]. The former can produce mechanical oscillation while the latter can deteriorate the system efficiency and the tracking accuracy.

Some methods have been proposed to reduce the affections of parameter differences for DBPC [29]–[32]. A current integral loop parallelly operates with the predictive control loop of PMSM drives to compensate the current error caused by parameter uncertainties [29]. In [30], the d-axis voltage is compensated by the integral of the d-axis current feedback, and the permanent-magnet flux is adjusted by the q-axis current feedback. However, the transient performances of DBPC are affected by integral loops [29], [30]. A parameter identification method is proposed in [31] based on a reconstruction characteristic vector from the disturbance observer with current injection. In [32], a novel current and disturbance observer is proposed to predict future stator currents and disturbances caused by model parameter algorithms. In [33], the inductance of PMSM is estimated by an extended state observer in DBPC, and the knowledge of permanent-magnet flux is not required since an incremental model is adopted. However, these observer-based methods increase the complexity of DBPC and the accuracy of observers also can affect the performances of DBPC.

In this paper, a hybrid dual-mode control (HDMC) is proposed for surface-mounted PMSM drives. The proposed HDMC contains two control modes (DBPC and FOC), and they are respectively employed in the transient operation and the steady-state operation. The proposed HDMC inherits the fast transient performances of DBPC and the good steady-state performances of FOC. Especially, no observer is required in the proposed HDMC and the static current error can be eliminated. The main challenge of the proposed HDMC is how to realize the optimal and smooth transition between DBPC and FOC while the performances are satisfactory during the entire operation. The paper is organized as follows. The studied PMSM drive is described in Section II. The so-called HDMC is proposed in Section III. Experiments are carried out in Section IV to verify the proposed hybrid control scheme. Finally, some conclusions are drawn in Section V.

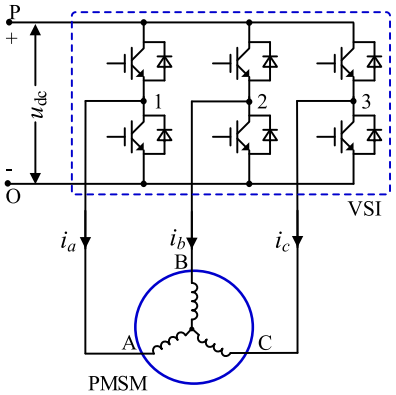

FIGURE 1. Studied PMSM drive system.

II. STUDIED PMSM DRIVE

A. SYSTEM DESCRIPTION

The studied PMSM drive system is shown in Fig. 1, in which a three-phase surface-mounted PMSM is controlled by a two-level three-leg VSI.

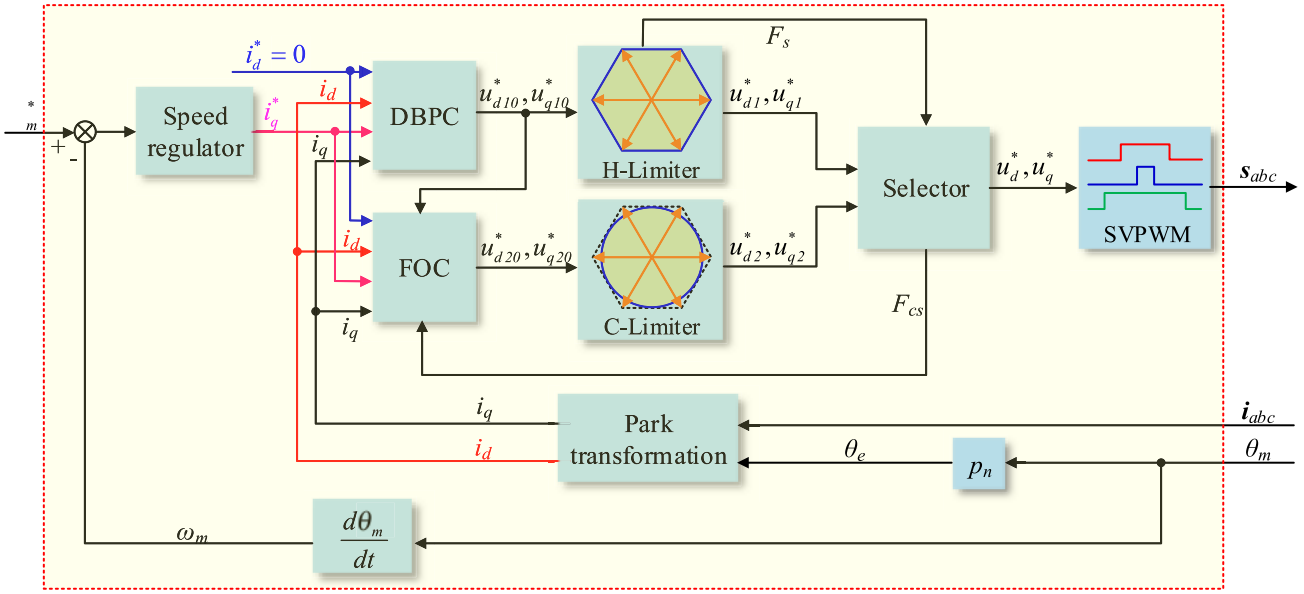

FIGURE 2. Block diagram of the proposed HDMC.

B. MATHEMATICAL MODEL OF PMSM

The voltage equation in dq coordinate system is expressed as

$$\begin{cases} u_d = R_s i_d + L_s \dfrac{di_d}{dt} - \omega_e L_s i_q \\ u_q = R_s i_q + L_s \dfrac{di_q}{dt} + \omega_e (L_s i_d + \psi_f) \end{cases} \tag{1}$$

where u_d and u_q are the d- and q-axis voltages, respectively; i_d and i_q are the d- and q-axis currents, respectively; R_s, L_s and ψ_f are the stator resistance, the stator inductance and the permanent-magnet flux linkage, respectively; ω_e is the electrical angular speed.

Due to the fact that the sampling period T_s is short, current differentiation can be rewritten as

$$\frac{di(k)}{dt} \approx \frac{i(k+1) - i(k)}{T_s} \tag{2}$$

where $i(k)$ is the current in the k^{th} sampling period.

Substituting (2) into (1) gives the discrete time state-space model of PMSM as

$$\begin{bmatrix} i_d(k+1) \\ i_q(k+1) \end{bmatrix} = \boldsymbol{P} \begin{bmatrix} i_d(k) \\ i_q(k) \end{bmatrix} + \boldsymbol{M} \begin{bmatrix} u_d(k) \\ u_q(k) \end{bmatrix} - \boldsymbol{Q} \tag{3}$$

with

$$\boldsymbol{P} = \begin{bmatrix} 1 - \dfrac{R_s T_s}{L_s} & T_s \omega_e \\ -T_s \omega_e & 1 - \dfrac{R_s T_s}{L_s} \end{bmatrix},$$

$$\boldsymbol{M} = \begin{bmatrix} \dfrac{T_s}{L_s} & 0 \\ 0 & \dfrac{T_s}{L_s} \end{bmatrix}, \quad \boldsymbol{Q} = \begin{bmatrix} 0 \\ \dfrac{T_s \omega_e \psi_f}{L_s} \end{bmatrix}$$

III. PROPOSED HDMC

The proposed HDMC is illustrated in Fig. 2, which mainly contains six modules: DBPC module, FOC module, H-Limiter module, C-Limiter module, Selector module, and SVPWM module. All modules are described in this section.

A. DBPC MODULE

In this module, the initial reference d-axis voltage $u_{d10}^*(k)$ and q-axis voltage $u_{q10}^*(k)$ are calculated according to the DBPC method, and the constraints of VSI is neglected. The theoretical control target of DBPC is to achieve both reference d-axis current $i_d^*(k)$ and q-axis current $i_q^*(k)$ in one sampling period, that is,

$$\begin{cases} i_d(k+1) = i_d^*(k) \\ i_q(k+1) = i_q^*(k) \end{cases} \tag{4}$$

In this paper, the reference d-axis current $i_d^*(k)$ is always 0 since $i_d = 0$ control is adopted. The reference q-axis current $i_q^*(k)$ is obtained by the speed regulator, where a PI controller is adopted. In order to realize the theoretical control target of DBPC, the initial reference d-axis voltage $u_{d10}^*(k)$ and q-axis voltage $u_{q10}^*(k)$ are calculated by substituting (4) into (3)

$$\begin{bmatrix} u_{d10}^*(k) \\ u_{q10}^*(k) \end{bmatrix} = \boldsymbol{M}^{-1} \left(\begin{bmatrix} i_d^*(k) \\ i_q^*(k) \end{bmatrix} - \boldsymbol{P} \begin{bmatrix} i_d(k) \\ i_q(k) \end{bmatrix} + \boldsymbol{Q} \right) \tag{5}$$

B. H-LIMITER MODULE

The magnitude of the initial reference voltage vector $\boldsymbol{V}_{\text{ref10}}$ is defined as

$$V_{ref\,10} = \sqrt{(u_{d10}^*)^2 + (u_{q10}^*)^2} \tag{6}$$

where V_{ref10} is the magnitude of $\boldsymbol{V}_{\text{ref10}}$. As is known, the output voltage ability of VSI is limited by the dc bus voltage u_{dc},

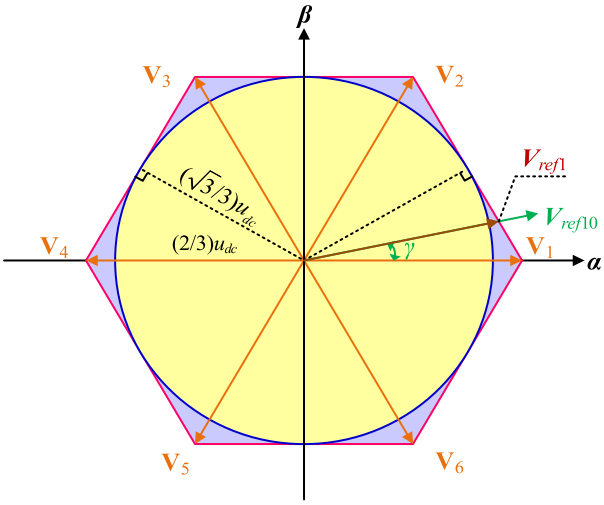

FIGURE 3. Voltage trajectories.

and the maximum voltage trajectory of VSI is hexagon, as shown in Fig. 3. In this paper, the phase angle of $\boldsymbol{V}_{\text{ref10}}$ is defined as γ, and the corresponding limitation value V_m can be calculated by

$$V_m = \frac{\sqrt{3}u_{dc}}{3\cos[\frac{\pi}{6} - (\gamma \bmod \frac{\pi}{3})]} \tag{7}$$

In DBPC module, the calculations of u^*_{d10} and u^*_{q10} do not consider the constraints of VSI. However, the implementation of $\boldsymbol{V}_{\text{ref10}}$ may be impossible due to the constraints of VSI. Therefore, the constraints of VSI are taken into account in this module.

Usually, the reference d-axis current i^*_d can be well achieved since its value always remains zero, and the difference Δi_d between the reference d-axis current i^*_d and the actual d-axis current i_d can be neglected. Furthermore, u^*_{d10} should be small according to (5).

At the beginning of the transient procedure, the difference Δi_q between the reference q-axis current i^*_q and the actual q-axis current i_q usually is large. Therefore, u^*_{q10} is significantly larger than u^*_{d10}. If V_{ref10} is larger than the limitation value V_m, the initial reference voltage vector $\boldsymbol{V}_{\text{ref10}}$ cannot be implemented and i^*_q cannot be achieved in one sampling period. Therefore, maximum voltage of VSI should be outputted to shorten the response time, and this situation is defined as the saturation state of VSI. A saturation flag F_s is defined as (8) in this paper, and it is set as 1 to indicate the saturation state.

$$F_s = \begin{cases} 1 & \text{if } V_{ref\,10} > V_m \\ 0 & \text{if } V_{ref\,10} \le V_m \end{cases} \tag{8}$$

Considering the constraints of VSI, the final reference voltage vector $\boldsymbol{V}_{\text{ref1}}$ can be modified as

$$\begin{cases} u^*_{d1} = V_m u^*_{d10}/V_{ref\,10} \\ u^*_{q1} = V_m u^*_{q10}/V_{ref\,10} \end{cases} \tag{9}$$

Obviously, the output voltage of VSI is mainly assigned to the q-axis voltage in the transient procedure. In other words, $\left|u^*_{q1}\right|$ is nearly equal to V_m, which does not affected by PMSM parameter variations during the transient procedure.

Gradually, the q-axis current difference Δi_q will become small, and then the reference q-axis current i^*_q can be achieved in one sampling period. In this situation, it is not necessary to output maximum voltage for VSI. Therefore, this situation is defined as the unsaturation state of VSI, and the saturation flag F_s is set as 0. In this situation, V_{ref10} is not larger than the limitation value V_m, and the final reference voltage vector $\boldsymbol{V}_{\text{ref1}}$ can be directly determined as

$$\begin{cases} u^*_{d1} = u^*_{d10} \\ u^*_{q1} = u^*_{q10} \end{cases} \tag{10}$$

However, the static current error will occur due to the existence of the PMSM parameter variations, as shown in Fig. 4.

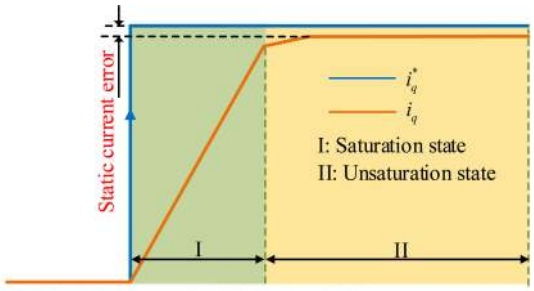

FIGURE 4. Variation procedure of i_q using DBPC.

As is seen in Fig. 4, the current variation rate in the saturation state is larger than that in the unsaturation state. It also can be found that most of q-axis current difference can be removed in the saturation state.

C. FOC MODULE

In this module, the initial reference d-axis voltage u^*_{d20} and q-axis voltage u^*_{q20} are obtained by two PI current regulators, respectively. The detailed block diagram of the FOC module is illustrated in Fig. 5. As is presented in DBPC module, however, u^*_{d10} and u^*_{q10} are directly calculated by DBPC according to (5). When the HDMC is switched from DBPC to FOC, the switching chattering may occur if the differences between (u^*_{d10}, u^*_{q10}) and (u^*_{d20}, u^*_{q20}) cannot be avoided. In order to avoid the switching chattering, u^*_{d20} and u^*_{q20} are respectively initialized by u^*_{d10} and u^*_{q10}, which are calculated by DBPC module at the trailing edge of the control scheme flag F_{cs}, which will be explained in Selector module.

The whole variation procedure of the actual q-axis current i_q using FOC is curved in Fig. 6. Due to the existence of PI current controllers in FOC, the current overshoot occurs and the torque (current) response is slower.

D. C-LIMITER MODULE

u^*_{d20} and u^*_{q20} are limited by C-Limiter module. In order to eliminate the static current error, FOC is implemented in

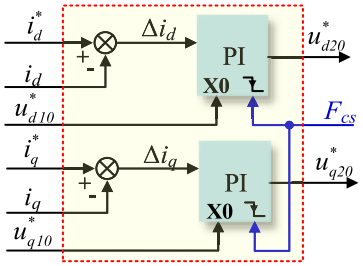

FIGURE 5. Block diagram of FOC module.

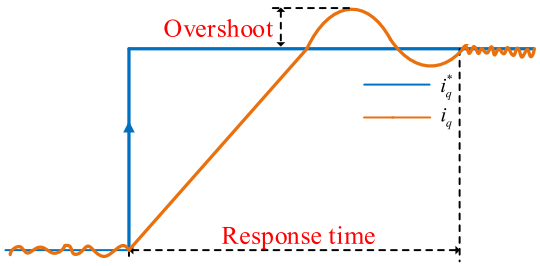

FIGURE 6. Variation procedure of i_q using FOC.

the steady-state operation. As is shown in Fig. 3, the maximum magnitude of the actual voltage vector varies from $(\sqrt{3}/3)u_{\rm dc}$ to $(2/3)u_{\rm dc}$ if the hexagon voltage trajectory is used for VSI. However, u_{d20}^* and u_{q20}^* should be constant in the steady-state operation according to (1). Hence, the magnitude of the reference voltage vector $\boldsymbol{V}_{\rm ref2}$ should be constant in the steady-state operation, which cannot be satisfied in the blue region shown in Fig. 3. In order to well remain the steady-state operation, the inscribed circle of the hexagon voltage trajectory is used for FOC module as shown in Fig. 3.

Referring to (6), the magnitude of the initial reference voltage vector $\boldsymbol{V}_{\rm ref20}$ can be calculated. If $V_{\rm ref20}$ is larger than $(\sqrt{3}/3)u_{\rm dc}$, the final reference voltage vector $\boldsymbol{V}_{\rm ref2}$ is respectively determined as

$$\begin{cases} u_{d2}^* = \dfrac{\sqrt{3}u_{dc}u_{d20}^*}{3V_{ref}} \\ u_{q2}^* = \dfrac{\sqrt{3}u_{dc}u_{q20}^*}{3V_{ref}} \end{cases} \tag{11}$$

Otherwise, u_{d20}^* and u_{q20}^* are respectively set as the values of u_{d2}^* and u_{q2}^*.

E. SELECTOR MODULE

In this module, $\boldsymbol{V}_{\rm ref1}$ from DBPC module or $\boldsymbol{V}_{\rm ref2}$ from FOC module is selected as the final reference voltage vector $\boldsymbol{V}_{\rm ref}$ for SVPWM module. The task of the HDMC is to inherit the quick torque response ability of DBPC but eliminate the static current error by using FOC. The main challenge of the proposed HDMC is how to appropriately assign the implementation time for DBPC and FOC modes.

If a new reference q-axis current i_q^* is set, the q-axis current difference Δi_q will become large, and VSI will immediately come into the saturation state ($F_{\rm s} = 1$). After several sampling periods, the q-axis current difference Δi_q can be gradually decreased, and finally VSI can come into the unsaturation state ($F_{\rm s} = 0$). According to the definition of the unsaturation state, the q-axis current difference Δi_q can be theoretically eliminated in one-sampling-period implementation of DBPC in the unsaturation state. After this sampling period, the transient procedure of the studied PMSM drive system can be theoretically considered to be completed, and the task of the HDMC becomes to remain the good steady-state operation. However, the q-axis current difference Δi_q usually cannot be eliminated by DBPC mode due to the PMSM parameter variations, and the static q-axis current error will occur if DBPC mode is still implemented after this sampling period. In order to eliminate the static current error in time, the FOC mode is adopted after this sampling period. The transition procedure from DBPC mode to FOC mode is demonstrated in Fig. 7. In the proposed HDMC, the control scheme flag $F_{\rm cs}$ is set as 1 if the DBPC mode is selected; otherwise, $F_{\rm cs}$ is set as 0.

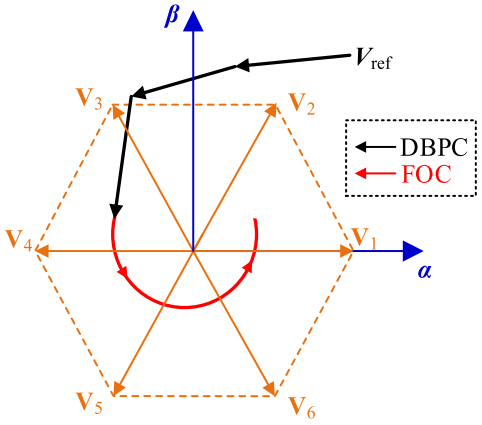

FIGURE 7. Transition procedure from DBPC to FOC.

Once VSI returns to the saturation state (F_s =1), it means that the q-axis current difference Δi_q become large, and the DBPC mode is selected again instead of the FOC mode to enhance the torque response ability of the proposed HDMC.

The flowchart of Selector module is illustrated in Fig. 8, in which N represents the number of sampling periods in unsaturation state using the DBPC mode.

F. SVPWM MODULE

According to SVPWM method, u_d^* and u_q^* can be implemented by generating the switch states $\boldsymbol{s}_{abc}$ for VSI in this module.

G. ENTIRE MODULE

The entire operation procedure of the proposed HDMC is illustrated in Fig. 9. As is shown in Fig. 9, the q-axis current difference $\Delta i_{\rm q}$ is mainly removed by the DBPC mode, and the steady-state operation of the studied PMSM drive system is remained by the FOC mode.

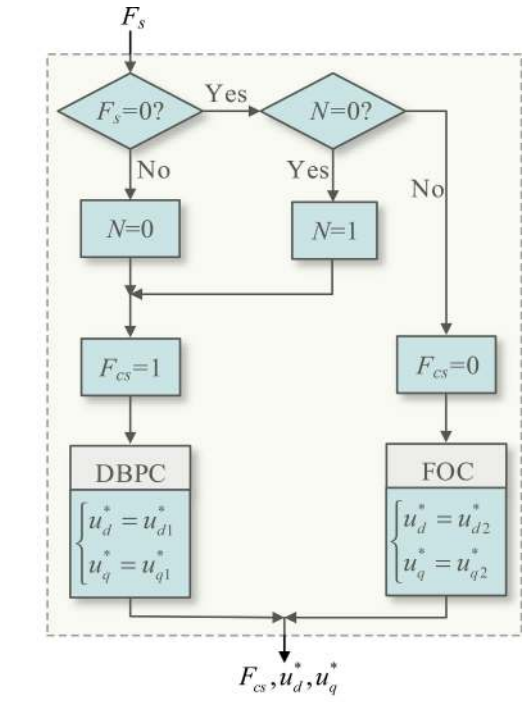

FIGURE 8. Flowchart of Selector module.

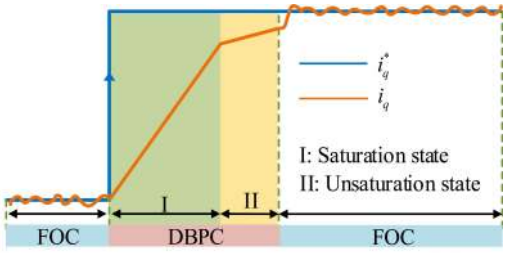

FIGURE 9. Variation procedure of i_q using the proposed HDMC.

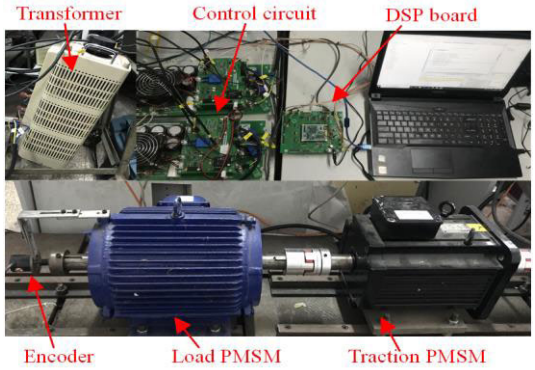

FIGURE 10. Experimental platform.

IV. EXPERIMENTAL VALIDATION

To verify the effectiveness of the proposed HDMC, an experiment platform is developed, as shown in Fig. 10. The studied PMSM is controlled by one three-leg VSI and its parameters are listed in TABLE 1. The load is provided by another PMSM with an encoder of 1024 pulses per revolution, and it is realized by the closed-loop torque control. The control program is implemented in a DSP TMS32028377 controller. The inputs for DSP controller are the measured phase currents and dc bus voltage, and the feedback signal of the encoder. The switch states for the VSI are generated by the DSP controller. The sampling frequency is 10 kHz. The dc bus voltage is 300 V, which is provided by a three-phase rectifier. In all experiments, stator inductance is set as 50% of rated value and PM flux linkage is set as 150% of rated value. In this paper, the response time of q-axis current is defined as the duration from the establishment of new reference currents to the steady-state actual currents with ±5% error band.

TABLE 1. Parameters of studied PMSM.

Parameter	Value
Rated phase current	11 A
Stator resistance R_s	0.665 Ω
Stator inductance L_s	7.93 mH
Permanent magnet flux ψ_f	0.299 Wb
Number of pole pairs P_n	4

A. DBPC

In this experiment, only DBPC is implemented during the entire operation, and the experimental results are shown in Fig. 11. In this experiment, the reference speed was changed between 200 r/min and 600 r/min. As seen in Fig. 11(a), the static current errors of d- and q-axis under 600 r/min are respectively 0.32 A and 1.03 A, and those under 200 r/min are respectively nearly 0 and 0.22 A, which are resulted by the parameter variation of PMSM. Obviously, the static current error of d-axis is smaller than that of q-axis, and the static current error will become larger if the speed increases. More explanations can be found in [30]. The rising and falling times of the actual q-axis current i_q are 0.70 ms, which are respectively shown in Figs. 11(b) and (c). It can be seen that DBPC performs quick torque (current) response but suffers from the static current errors.

B. FOC

In this experiment, only FOC is implemented during the entire operation, and the experimental results are shown in Fig. 12. In this experiment, the reference speed was also changed between 200 r/min and 600 r/min. It can be seen that the static current errors can be eliminated by FOC. The rising and falling time of i_q are respectively 4.20 ms and 8.40 ms. Obviously, the torque (current) response of FOC is much slower than that of DBPC. Meanwhile, current overshoots occur in the transient procedures of FOC, and the current overshoot in the rising procedure is 2.06 A while that in the falling procedure is 2.67 A. However, current overshoots do not exist in DBPC.

C. HDMC

In this experiment, the proposed HDMC is implemented during the entire operation, and the experimental results are shown in Fig. 13. The rising and falling times of i_q is

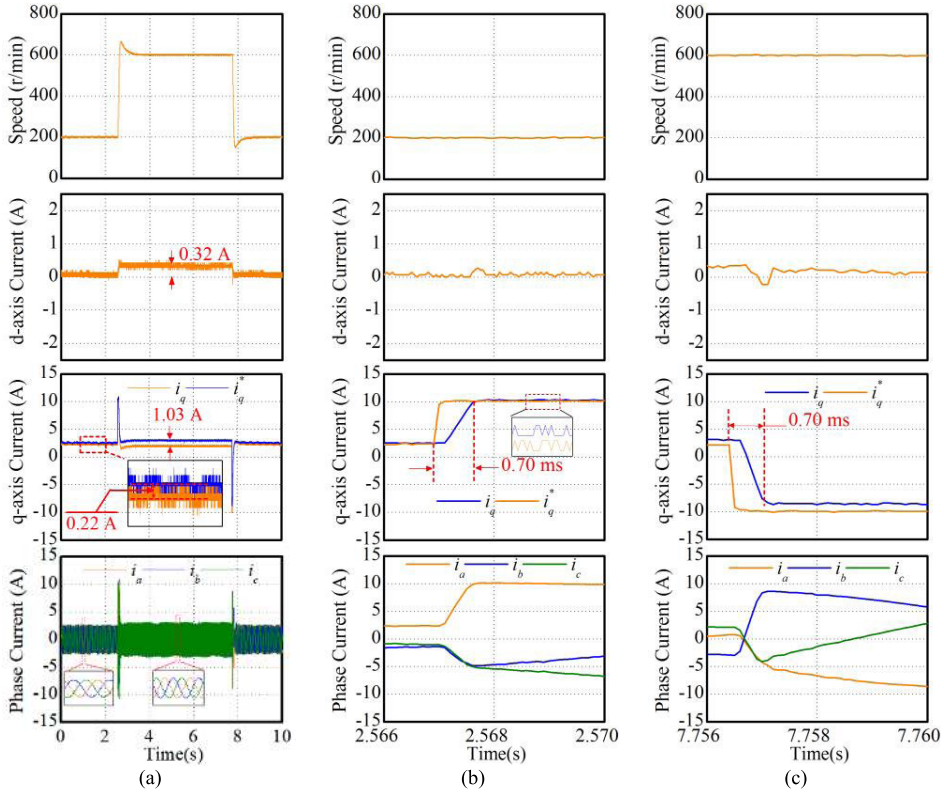

FIGURE 11. Experimental results of DBPC scheme: (a) t = 0-10 s, (b) t = 2.566-2.570 s, (c) t = 7.756-7.764 s.

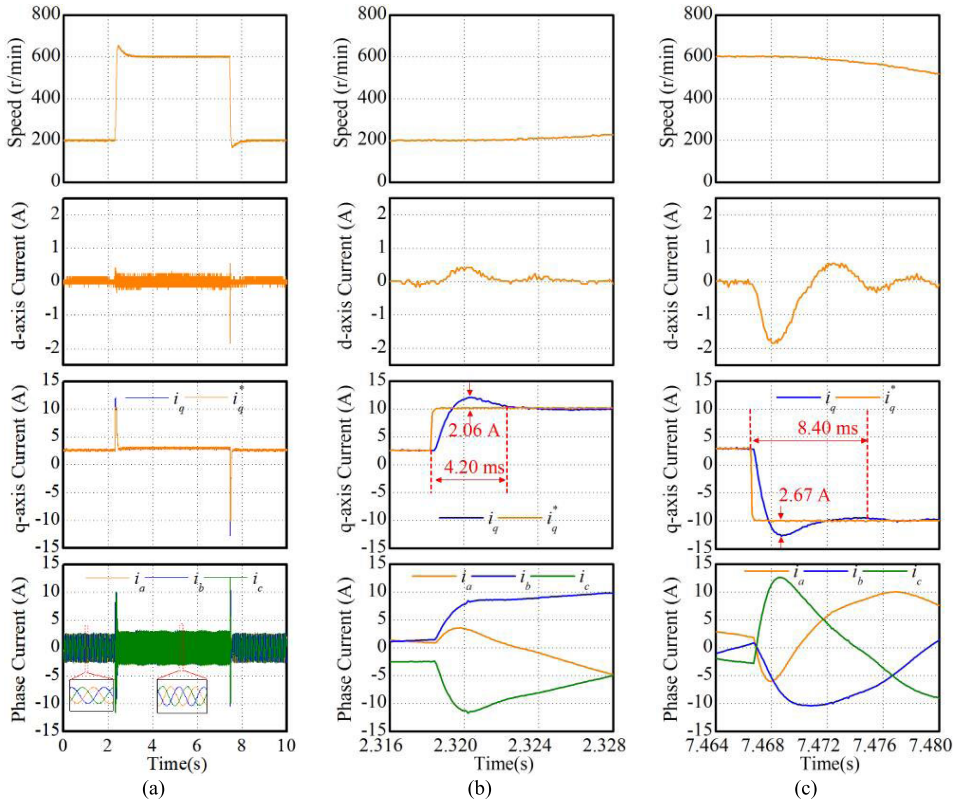

FIGURE 12. Experimental results of FOC scheme. (a) t = 0-10 s, (b) t = 2.316-2.328 s, (c) t = 7.464-7.480 s.

respectively 0.70 ms and 1.60 ms. The performance comparison of different control schemes is listed in TABLE 2.

Comparing with Fig. 11, the rising time of the proposed HDMC is as same as that of DBPC but the falling time of the

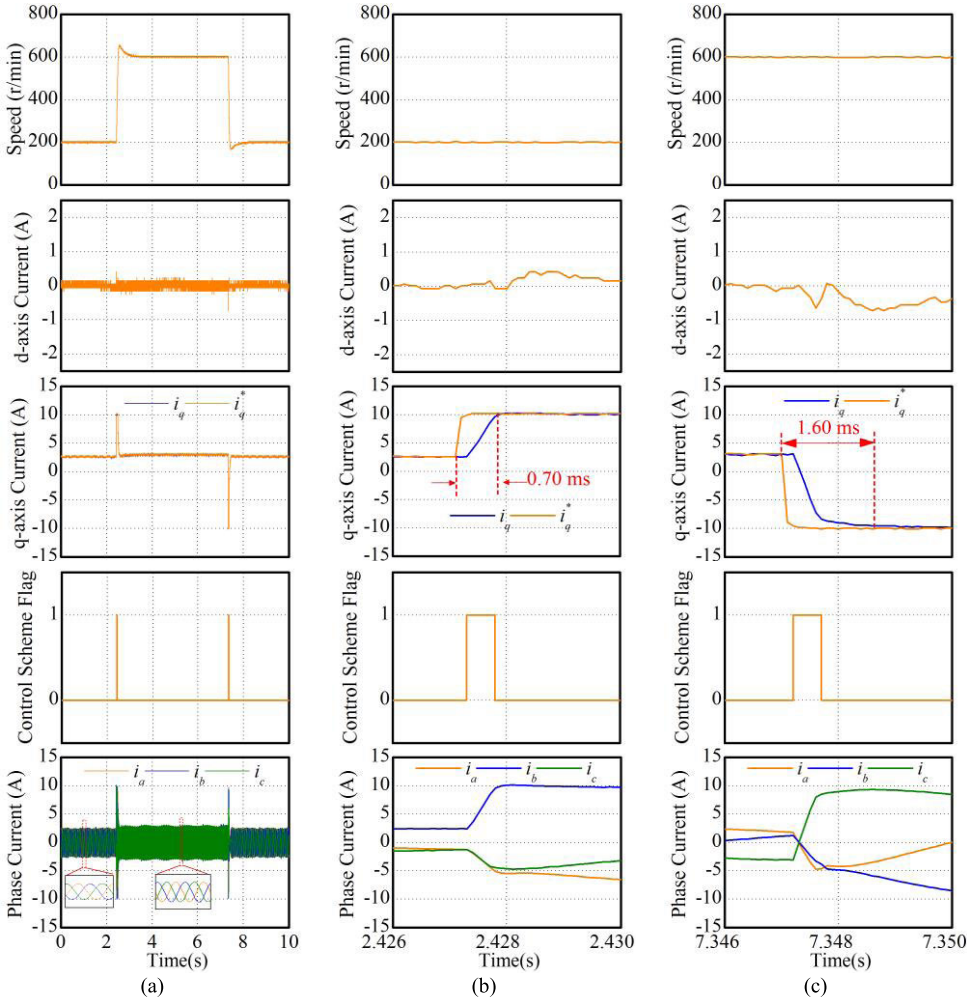

FIGURE 13. Experimental results of the proposed HDMC. (a) t = 0-10 s, (b) t = 2.426-2.430 s, (c) t = 7.346-7.350 s.

TABLE 2. Performance comparison of difference methods.

	Static error	Current response	Current overshoot
DBPC	bad	good	good
FOC	good	bad	bad
HDMC	good	medium	good

proposed HDMC seems to be significantly longer than that of DBPC. The reason is that the q-axis static current error in the rising procedure is small (0.22 A, as shown in Fig. 11) while that in the falling procedure is large (1.03 A, as shown in Fig. 11). The q-axis static current errors are eliminated by the FOC mode. The regulation time to eliminate the q-axis static current error in the rising procedure is so short that it does not affect the rising time. According to the curve of the control scheme flag F_{cs}, and the DBPC mode is nearly implemented in the entire rising procedure. However, the regulation time to eliminate the q-axis static current error in the falling procedure is so long that the falling time is seriously affected. According to the curve of the control scheme flag F_{cs}, the implementation time of the FOC mode is so long in the rising procedure that it cannot be neglected. The steady-state q-axis current after the falling procedure is 8.97 A in Fig. 11. For fair comparison, the steady-state q-axis current after the falling procedure is also assumed to be 8.97 A in Fig. 13. Based on this assumption, the modified falling time in Fig. 13 is also 0.7 ms. The adding response time (0.9 ms) is the regulation time to eliminate the static current error (1.03 A). Therefore, HDMC has same response ability of DBPC.

Comparing with Fig. 12, the torque (current) response of the proposed HDMC is significantly better than that of FOC but the current overshoot has been significantly suppressed. The explanation is that the current transient response is mostly completed by DBPC module and only the final step is implemented with FOC, as shown in Fig. 8.

V. CONCLUSION

In this paper, HDMC is proposed for the surface-mounted PMSM drive, which inherits the quick response ability of DBPC but eliminates the static current error by using FOC. The DBPC mode is activated immediately once VSI comes

into the saturation state. After one-sampling-period implementation of the DBPC mode in the unsaturation state, the FOC mode is activated to eliminate the static current error since most of the current difference has been removed by the DBPC mode. In order to avoid the switching chattering, the PI current controllers in the FOC mode are initialized by the desired voltage vector calculated in the transition period. The effectiveness of HDMC is verified by experimental results.

REFERENCES

[1] M. Cheng, W. Hua, J. Zhang, and W. Zhao, "Overview of stator-permanent magnet brushless machines," *IEEE Trans. Ind. Electron.*, vol. 58, no. 11, pp. 5087–5101, Nov. 2011.
[2] P.-Y. Chen, K.-W. Hu, Y.-G. Lin, and C.-M. Liaw, "Development of a prime mover emulator using a permanent-magnet synchronous motor drive," *IEEE Trans. Power Electron.*, vol. 33, no. 7, pp. 6114–6125, Jul. 2018.
[3] W. Wang, Y. Feng, Y. Shi, M. Cheng, W. Hua, and Z. Wang, "Direct thrust force control of primary permanent-magnet linear motors with single DC-link current sensor for subway applications," *IEEE Trans. Power Electron.*, vol. 35, no. 2, pp. 1365–1376, Feb. 2020.
[4] W. Tong, S. Dai, S. Wu, and R. Tang, "Performance comparison between an amorphous metal PMSM and a silicon steel PMSM," *IEEE Trans. Magn.*, vol. 55, no. 6, pp. 1–5, Jun. 2019.
[5] Z. Shen, D. Jiang, L. Zhu, Y. Xu, T. Zou, Z. Liu, and R. Qu, "A novel zero-sequence current elimination PWM scheme for an open-winding PMSM with common DC bus," *IEEE Trans. Power Electron.*, vol. 34, no. 12, pp. 12476–12490, Dec. 2019.
[6] B. K. Bose, *Modern Power Electronics and AC Drives*. Upper Saddle River, NJ, USA: Prentice-Hall, 2002.
[7] W. Wang, Y. Feng, Y. Shi, M. Cheng, W. Hua, and Z. Wang, "Fault-tolerant control of primary permanent-magnet linear motors with single phase current sensor for subway applications," *IEEE Trans. Power Electron.*, vol. 34, no. 11, pp. 10546–10556, Nov. 2019.
[8] T. Sun, J. Wang, A. Griffo, and B. Sen, "Active thermal management for interior permanent magnet synchronous machine (IPMSM) drives based on model predictive control," *IEEE Trans. Ind. Appl.*, vol. 54, no. 5, pp. 4506–4514, Sep. 2018.
[9] A. A. Ahmed, B. K. Koh, and Y. I. Lee, "A comparison of finite control set and continuous control set model predictive control schemes for speed control of induction motors," *IEEE Trans. Ind. Informat.*, vol. 14, no. 4, pp. 1334–1346, Apr. 2018.
[10] H. A. Young, M. A. Perez, and J. Rodriguez, "Analysis of finite-control-set model predictive current control with model parameter mismatch in a three-phase inverter," *IEEE Trans. Ind. Electron.*, vol. 63, no. 5, pp. 3100–3107, May 2016.
[11] Y. Luo and C. Liu, "Model predictive control for a six-phase PMSM motor with a reduced-dimension cost function," *IEEE Trans. Ind. Electron.*, vol. 67, no. 2, pp. 969–979, Feb. 2020.
[12] P. Cortes, M. P. Kazmierkowski, R. M. Kennel, D. E. Quevedo, and J. Rodriguez, "Predictive control in power electronics and drives," *IEEE Trans. Ind. Electron.*, vol. 55, no. 12, pp. 4312–4324, Dec. 2008.
[13] R. O. Ramirez, J. R. Espinoza, F. Villarroel, E. Maurelia, and M. E. Reyes, "A novel hybrid finite control set model predictive control scheme with reduced switching," *IEEE Trans. Ind. Electron.*, vol. 61, no. 11, pp. 5912–5920, Nov. 2014.
[14] H. T. Nguyen and J.-W. Jung, "Finite control set model predictive control to guarantee stability and robustness for surface-mounted PM synchronous motors," *IEEE Trans. Ind. Electron.*, vol. 65, no. 11, pp. 8510–8519, Nov. 2018.
[15] W. Wang, J. Zhang, and M. Cheng, "Common model predictive control for permanent-magnet synchronous machine drives considering single-phase open-circuit fault," *IEEE Trans. Power Electron.*, vol. 32, no. 7, pp. 5862–5872, Jul. 2017.
[16] Y. Guo, J. Si, C. Gao, H. Feng, and C. Gan, "Improved fuzzy-based Taguchi method for multi-objective optimization of direct-drive permanent magnet synchronous motors," *IEEE Trans. Magn.*, vol. 55, no. 6, Jun. 2019, Art. no. 8102204.
[17] A. Soualhi, G. Clerc, and H. Razik, "Detection and diagnosis of faults in induction motor using an improved artificial ant clustering technique," *IEEE Trans. Ind. Electron.*, vol. 60, no. 9, pp. 4053–4062, Sep. 2013.
[18] X. Zhang, L. Zhang, and Y. Zhang, "Model predictive current control for PMSM drives with parameter robustness improvement," *IEEE Trans. Power Electron.*, vol. 34, no. 2, pp. 1645–1657, Feb. 2019.
[19] T. Tao, W. Zhao, Y. Du, Y. Cheng, and J. Zhu, "Simplified fault-tolerant model predictive control for a five-phase permanent-magnet motor with reduced computation burden," *IEEE Trans. Power Electron.*, vol. 35, no. 4, pp. 3850–3858, Apr. 2020.
[20] K. Drobnic, M. Nemec, D. Nedeljkovic, and V. Ambrozic, "Predictive direct control applied to AC drives and active power filter," *IEEE Trans. Ind. Electron.*, vol. 56, no. 6, pp. 1884–1893, Jun. 2009.
[21] X. Yuan, C. Zhang, and S. Zhang, "A novel deadbeat predictive current control scheme for OEW-PMSM drives," *IEEE Trans. Power Electron.*, vol. 34, no. 12, pp. 11990–12000, Dec. 2019.
[22] J. Zhao, L. Zheng, S. Wang, and M. Hua, "Research on deadbeat current prediction vector control system of axial flux permanent magnet synchronous motor for electric bus based on efficiency optimal torque distribution method," *IEEE Access*, vol. 7, pp. 128384–128393, 2019.
[23] S. A. Davari, F. Wang, and R. M. Kennel, "Robust deadbeat control of an induction motor by stable MRAS speed and stator estimation," *IEEE Trans. Ind. Informat.*, vol. 14, no. 1, pp. 200–209, Jan. 2018.
[24] Y. Jiang, W. Xu, C. Mu, and Y. Liu, "Improved deadbeat predictive current control combined sliding mode strategy for PMSM drive system," *IEEE Trans. Veh. Technol.*, vol. 67, no. 1, pp. 251–263, Jan. 2018.
[25] C. Xu, Z. Han, and S. Lu, "Deadbeat predictive current control for permanent magnet synchronous machines with closed-form error compensation," *IEEE Trans. Power Electron.*, vol. 35, no. 5, pp. 5018–5030, May 2020, doi: 10.1109/TPEL.2019.2943016.
[26] S.-W. Kang, J.-H. Soh, R.-Y. Kim, K.-J. Lee, and S.-I. Kim, "Robust predictive current control for IPMSM without rotor flux information based on a discrete-time disturbance observer," *IET Electr. Power Appl.*, vol. 13, no. 12, pp. 2079–2089, Dec. 2019.
[27] M. Zafarani, T. Goktas, and B. Akin, "A comprehensive magnet defect fault analysis of permanent-magnet synchronous motors," *IEEE Trans. Ind. Appl.*, vol. 52, no. 2, pp. 1331–1339, Apr. 2016.
[28] X.-H. Jin, Y. Zhang, and D.-G. Xu, "Static current error elimination algorithm for induction motor predictive current control," *IEEE Access*, vol. 5, pp. 15250–15259, 2017.
[29] H. Le-Huy, K. Slimani, and P. Viarouge, "Analysis and implementation of a real-time predictive current controller for permanent-magnet synchronous servo drives," *IEEE Trans. Ind. Electron.*, vol. 41, no. 1, pp. 110–117, Feb. 1994.
[30] G. Wang, M. Yang, L. Niu, X. Gui, and D. Xu, "Improved predictive current control with static current error elimination for permanent magnet synchronous machine," in *Proc. 40th Annu. Conf. IEEE Ind. Electron. Soc. (IECON)*, Oct. 2014, pp. 661–667.
[31] Y. Yao, Y. Huang, F. Peng, J. N. Dong, and H. Zhang, "An improved deadbeat predictive current control with online parameter identification for surface-mounted PMSMs," *IEEE Trans. Ind. Electron.*, early access, Dec. 24, 2019, doi: 10.1109/TIE.2019.2960755.
[32] X. Yuan, S. Zhang, and C. Zhang, "Enhanced robust deadbeat predictive current control for PMSM drives," *IEEE Access*, vol. 7, pp. 148218–148230, Jan. 2019.
[33] M. Yang, X. Lang, J. Long, and D. Xu, "Flux immunity robust predictive current control with incremental model and extended state observer for PMSM drive," *IEEE Trans. Power Electron.*, vol. 32, no. 12, pp. 9267–9279, Dec. 2017.

WEI WANG (Senior Member, IEEE) was born in Jiangsu, China. He received the B.Sc. degree in electrical engineering from the Nanjing University of Science and Technology, Nanjing, China, in 2008, and the Ph.D. degree in electrical engineering from Southeast University, Nanjing, China, in 2014, respectively.

Since 2014, he has been with Southeast University, where he is currently an Associate Professor with the School of Electrical Engineering. He was a Joint Ph.D. Student with the University of Lille 1, Lille, France. He is the author or coauthor of more than 30 technical articles. His research interests include motor drives and traction system for rail transit. From October 2011 to October 2012, he received the scholarship from China Scholarship Council.

ZHIXIANG LU was born in Jiangsu, China. He received the B.Sc. degree in electrical engineering from the Nanjing University of Science and Technology, Nanjing, China, in 2018. He is currently pursuing the M.Sc. degree in electrical engineering with Southeast University, Nanjing.

His current research interest includes high-performance controls of permanent-magnet motor drives.

WEI HUA (Senior Member, IEEE) was born in Taizhou, China, in 1978. He received the B.Sc. and Ph.D. degrees in electrical engineering from Southeast University, Nanjing, China, in 2001 and 2007, respectively.

Since 2007, he has been with Southeast University, where he is currently a Professor with the School of Electrical Engineering. He is the author or coauthor of more than 100 technical articles. He is the holder of 44 patents in his areas of interest. His teaching and research interests include the design, analysis, and control of electrical machines.

ZHENG WANG (Senior Member, IEEE) received the B.Eng. and M.Eng. degrees from Southeast University, Nanjing, China, in 2000 and 2003, respectively, and the Ph.D. degree from The University of Hong Kong, Hong Kong, in 2008.

From 2008 to 2009, he was a Postdoctoral Fellow with Ryerson University, Toronto, ON, Canada. He is currently a Full Professor with the School of Electrical Engineering, Southeast University, China. His research interests include electric drives, power electronics, and distributed generation. He has authored or coauthored over 80 internationally refereed articles and four books in these areas. He received several academic awards including the IEEE PES Chapter Outstanding Engineer Award, the Best Paper Award of International Conference on Electrical Machines and Systems (ICMES), the Best Session Paper Award of IEEE Annual Meeting of Industrial Electronics (IECON), and the Nanjing Outstanding Paper Award of Natural Science.

MING CHENG (Fellow, IEEE) received the B.Sc. and M.Sc. degrees from the Department of Electrical Engineering, Southeast University, Nanjing, China, in 1982 and 1987, respectively, and the Ph.D. degree from the Department of Electrical and Electronic Engineering, The University of Hong Kong, Hong Kong, in 2001.

Since 1987, he has been with Southeast University, where he is currently a Distinguished Professor with the School of Electrical Engineering and the Director of the Research Center for Wind Power Generation. From January to April 2011, he was a Visiting Professor with the Wisconsin Electric Machine and Power Electronics Consortium, University of Wisconsin, Madison, WI, USA. His teaching and research interests include electrical machines, motor drives for EV, and renewable energy generation. He has authored or coauthored more than 300 technical article and four books. He is the holder of 70 patents in these areas.

Prof. Cheng is a Fellow of the Institution of Engineering and Technology. He has served as the Chair and an Organizing Committee Member for many international conferences. He is a Distinguished Lecturer of the IEEE Industry Applications Society, from 2015 to 2016.